2012-10-27

The Role of Case-Hardening in the Development and Preservation of Narrow, Vertical-Walled Canyons in Adršpach-Teplice, Czech Republic

Shawn Austin Wiggins
Brigham Young University - Provo

The Role of Case-Hardening in the Development and Preservation of Narrow, Vertical-Walled Canyons in Adršpach-Teplice, Czech Republic

Shawn A. Wiggins

A thesis submitted to the faculty of
Brigham Young University
in partial fulfillment of the requirements for the degree of

Master of Science

Alan L. Mayo, Chair
Thomas H. Morris
John H. McBride
Jani Radebaugh

Department of Geological Sciences

Brigham Young University

October 2012

ABSTRACT

The Role of Case-Hardening in the Development and Preservation of Narrow, Vertical-Walled Canyons in Adršpach-Teplice, Czech Republic

Shawn A. Wiggins
Department of Geological Sciences, BYU
Master of Science

The geomorphology at Adršpach-Teplice, Czech Republic is dominated by vertical-walled, fracture-controlled features including slot canyons, gorges and pillars. Surfaces of canyon walls in Adršpach are case-hardened and more resistant to erosion than the bulk of the sandstone, which appears to be fundamental to the formation and preservation of canyons. Core and whole rock samples from Adršpach-Teplice were analyzed in thin section, including SEM analysis with cathodo luminescence. XRF and XRD analyses indicated that silica case-hardened surfaces are chemically and mineralogically similar to the rock interior, while iron case-hardened surfaces have an increase in iron present at the surface as the mineral goethite. Permeability analysis indicates a decrease in porosity in case-hardened surfaces. The rock at Adršpach-Teplice is poorly cemented yet has the strength to maintain vertical faces because of a locked sand structure, which was formed by pressure solution. Fracture faces contain disaggregation and cataclastic bands that reduce porosity and increase strength. Case-hardening exists on fracture faces and other surfaces as either silica or iron. Silica case-hardening is ubiquitous in the area and consists of a slight increase in abundance of silica overgrowths and sometimes an increase in clay content. It can form on fresh surfaces in as little as five years, creating what is essentially a self-repairing material. Iron case-hardening is composed of goethite, is much less prevalent than silica case-hardening, and does not appear to be actively depositing. Lichens, fungi, and other biological material are present on case-hardened surfaces and may add to the strength of the material. The internal structure of the rock lends the strength to form and maintain the features seen at Adršpach-Teplice, while case-hardening helps to protect them from erosion.

Keywords: Case-hardening, Adršpach-Teplice, locked sand, pressure solution, sandstone, vertical-walled, rock city

TABLE OF CONTENTS

LIST OF FIGURES

LIST OF TABLES

INTRODUCTION

In the absence of fluvial erosion, weathering is commonly dominated by vadose and shallow groundwater processes (McFarlane, 1992). Fractures in bedrock do not have enough aperture to allow for physical erosion by fluvial processes, but do allow for fluid flow, which induces chemical weathering. This can involve both the dissolution and precipitation of rock-forming minerals. In some instances, minerals that are resistant to erosion precipitate on rock faces, a process known as case-hardening (Conca and Rossman, 1982). The presence of case-hardening may play an important part in the development of some slot canyons, and may be especially significant in the preservation of vertical walls (Viles and Goudie, 2004). Case-hardening is a fundamentally different process than the processes attributed to the creation of fluvial carved slot canyons, which are thought to be enlarged by flash-flooding (Carter and Anderson, 2006; Rogers and Engelder, 2004).

Several different mineral types have been observed to contribute to case-hardening, and can be deposited through a number of processes. Clay minerals can be deposited on rock faces by wind (Conca and Rossman, 1982) or aqueous deposition of atmospheric dust (Thiagarajan and Lee, 2004). Alternately, material can come from the interior of the rock and be precipitated on the surface due to evaporation (Adomovič et. al., 2011) or oxidation (Vařilová, 2007; Garvie et al., 2008). In some cases, many processes can simultaneously contribute to case-hardening. Desert varnish can be composed of amorphous silica deposited through evaporation (Perry et. al., 2006), clay from atmospheric dust, and oxidized manganese and iron (Potter and Rossman, 1977). Micro-organic biofilms can also aid in surface cementation (Viles et al., 2004).

This study will investigate the origin and effects of case-hardening near Adršpach-Teplice, Czech Republic (Figure 1), which appears to be important in the formation and preservation of rock city structures.

Purpose and Objectives

The primary purpose of this study is to determine the effect that case-hardening has on the formation and preservation of vertical-walled canyons. This will be accomplished through the following objectives:

1. Characterize the distribution and physical properties of surface coatings at Adršpach-Teplice.
2. Describe the chemistry and mineralogy of surface coatings and the underlying rock.
3. Understand the relationship between case-hardened fractures and slot canyon development.

GEOLOGIC SETTING

In northern and eastern Bohemia, Czech Republic, and in the northeastern-most portion of Germany, Cretaceous age (middle Turonian to early Coniacian), shallow marine sandstone of the Brezno Formation (Barnet and Burda, 1997; Uličný, 2001) crops out over large areas known as rock cities. Rock cities are characterized by narrow, steep-walled canyons and gorges 20-60m deep (Cílek and Žák, 2007) and 0.1-25 m wide. Case-hardening has been observed on rock faces throughout the Bohemian Cretaceous Basin. Several ideas have been proposed to explain the formation of the canyons and the case-hardened surfaces. Adamovič et al. (2011) suggest that silica crusts are the most common form of case-hardening and have precipitated through evaporation on and just

below rock surfaces. Iron-oxyhydroxides (primarily goethite) are also observed on rock faces and fractures. In a study in Bohemian Switzerland, northwest Czech Republic, Vařilová, (2007) suggests a hydrothermal origin, genetically linked to tertiary volcanism as the cause of the goethite case-hardening. Adamovič et al. (2011) and Přikyl et al. (2006) found that the pockmarks, tafoni, and honeycombing that are common on case-hardened surfaces in the Bohemian Cretaceous Basin result from salt weathering.

Although several ideas have been proposed for the origin of the silica and iron-oxide case-hardened surfaces, these surfaces have not been studied in detail. Both silica and iron oxide case-hardened surfaces are particularly well exposed on canyon wall faces in the Adršpach-Teplice region of the Czech Republic, in the Police basin near the Polish border (Figure 1). The rock city at Adršpach-Teplice covers ~16 km^2, but case-hardened vertical walls are especially well exposed in a ~0.13 km^2 area to the south known as Rock Island (Figure 2). The slot canyons at Adršpach form along closely-spaced joint patterns (Stejskal, 2005) in cross-bedded shallow marine sandstone that was deposited in a deltaic system (Uličný et al., 2009). Silica case-hardening is ubiquitous in the region, and iron case-hardening is also observed. Previous research in other rock cities in the Czech Republic has been undertaken to determine erosion rates of sandstone walls. This research has included ^{14}C and U-series dating of speleothems, studies in paleovegetation, and undisturbed archeological discoveries adjacent to sandstone walls. These studies suggest that there has not been lateral erosion or widening of the canyon walls for at least 10,000 years (Cilek and Zak, 2007; Kunes et al., 2007; Bruthans et al., 2009; Bruthans et al., 2012a). The canyon floors are generally flat and filled with sandy sediment. Though the area receives a substantial amount of precipitation and the climate is mild (mean

annual precipitation ~ 830 mm, average winter snow cover ~ 230 mm, and mean annual temperature ~6.5 ^{o}C) (Svoboda, 1970), there is no evidence of significant fluvial processes in the slot canyons.

METHODS

Core and whole rock samples were collected from an area of Adršpach known as Rock Island, from a cave approximately 1 km to the east, and at the north end of the park (Figure 3, Table 1). These areas were selected because of their prominent outcrops and relatively easy access. Samples collected from iron oxide and silica case-hardened surfaces were used for laboratory measures of porosity and permeability, for the preparation of thin sections, and for laboratory XRD, XRF, SEM and Microprobe analysis. Field XRF analysis was performed on both iron oxide and silica case-hardened surfaces using a portable XRF device.

Coring was attempted on cliff faces about 0.5-1.5 m above the ground surface using a hand-held gas-powered core driller with a 2.54 cm diameter diamond bit, using water as a coolant. Thirty-two cores were attempted, but due to the friability of the rock only two cores were recovered in the field that did not fracture and were of sufficient length for laboratory porosity and permeability testing (Table 2). Laboratory testing of permeability required cores a minimum of 3 cm long. Seven additional cores were recovered that were >3 cm long, but were fractured or partially disintegrated making them unusable for porosity and permeability. Twelve short cores, 0.5 – 2 cm long, were also obtained. These short cores are herein referred to as buttons, and each includes the case-hardened surface. Attempts were made to permeate rock faces with linseed oil and diluted wood glue prior to coring to prevent disintegration during coring. These methods

were not successful as the diluted wood glue would not permeate the rock and the linseed oil would not dry within the field schedule.

Five oriented whole rock samples were collected from Rock Island cliff faces and three samples were collected from the cave area for laboratory analysis (Table 1). From these samples, thirteen 2.54 cm diameter core samples were obtained in the laboratory using a drill press and liquid nitrogen as a coolant. One button was also recovered using this method. Four additional cores were attempted in the lab and yielded no recoverable material.

Porosity and permeability analyses were performed on the thirteen cores obtained in the laboratory as well as the two obtained in the field. Permeability was measured using a Temco/CLI Utra Perm 500 permeameter. Samples were analyzed with the case-hardened surface intact and then again after cutting off approximately 1 cm of material from the case-hardened surface. Samples ICS1 and TOC were insufficient in length and were only analyzed with the case-hardened surface intact. Porosity was measured using a Temco/CLI Ultrapore 300 porosimeter. All porosity analyses were performed after the case-hardened end was removed because the instrument required square-cut cores.

Twenty-two oriented thin sections were prepared from selected core and whole rock samples (Table 3). Each thin section was analyzed using a petrographic microscope. To better observe quartz overgrowths, six thin sections were polished for analysis with a scanning electron microscope (SEM) using cathodo luminescence. A total of 57 images were taken using the SEM. Four of those images were selected as representative of the typical quartz cementation. These were analyzed with ESRI's ArcGIS software. A line-type shape file was created to delineate the quartz grain boundaries, excluding quartz

overgrowths. Sections where quartz overgrowths contribute to cementation were differentiated and the percentage of cementation due to quartz overgrowths was calculated.

To understand the chemical components of the rock, eleven samples were analyzed using X-ray fluorescence (XRF). Six of these samples were prepared by separating the outer 1 cm from the interior of the rock and analyzing them separately. In samples where not enough material was available, only one analysis of the bulk rock was performed. Data was obtained using a Rigaku XRF.

Chemical data was also collected in the field using a Bruker Portable X-ray Fluorescence (pXRF) device. In-situ measurements were taken at 73 locations at or near Rock Island, with each measurement lasting 120 seconds. Fourteen of these measurements were taken on iron-coated surfaces, while the remaining 59 were taken on silica-coated surfaces.

Mineralogical data was obtained using RockJock11 (Eberl, 2003) on powder XRD patterns for six samples. These were the same samples that had their coating separated from their interior, and each was run separately.

Microprobe analysis was performed on polished thin sections. Using this method, it is possible to determine the chemistry of individual mineral grains and clays. Mineral grains analyzed were all quartz. Clays analyzed were composed of silica, aluminum, and sometimes potassium. Because this chemistry was also determined using the XRF, and mineralogical data for clays was determined using XRD, the microprobe data was deemed inferior for our purposes and was abandoned.

Fractures spacing and orientation were measured in the Rock Island area (Figure 2). Rock Island is roughly ellipsoidal in shape, with its major axis running approximately NE-SW. It is bounded by two perennial stream channels, with discharge rates of several liters per second. The dominant fracture orientation is NW-SE, with conjugate fractures oriented NE-SW. Only the dominant fractures were measured due to poor access to conjugate fractures. Measurements were taken on both the NW and SE sides of Rock Island. Strike was measured on a total of 387 fractures. The distance between these fractures was also measures. The type of coating on each fracture was recorded, along with general descriptions.

RESULTS

Dominant fractures in Rock Island are sub-vertical and have an average orientation of 145˚ (Figure 4). Distances between fractures range from 0.18 - 22.8 m, with an average spacing of 3.69 m. The largest fracture spacings (>15 m, with only two occurrences) probably encompass several parallel fractures that could not be observed due to vegetation and boulder fill.

Fracture faces were typically well preserved, with exposed faces (open fractures) maintaining their vertical orientation (Figure 5). In some areas, sapping and undercutting were observed. This was common where material was missing between two fractures, forming small slot canyons often filled with rectangular boulders (Figure 6). Other fractures have openings of only a few centimeters with very little exposure of the fracture faces (closed fractures) (Figure 7).

Silica and iron case-hardening are easily differentiated visually and were observed throughout rock island. Of the 387 fractures observed, all have what appears to be silica

case-hardening covering almost the entire fracture face. Silica case-hardened surfaces are only a few millimeters thick and are a slightly darker gray color than the interior of the rock, which typically has a tan color. Approximately 17% of the fractures also have iron oxide present at the surface. This is visible as a reddish-brown layer 0.5-2 cm thick that is usually patchy and was never observed to cover an entire fracture (Figure 8). In some cases, iron oxide was observed along nearly horizontal bedding surfaces. What appears to be silica case-hardening was also observed throughout the park, including on inscriptions in the stone reading "1882" and "1980" and on a surface exposed by quarrying five years prior to observation. Lichens and other biological material were also commonly observed on the case-hardened surfaces.

Visual analyses of core and whole rock samples indicate a composition of primarily quartz sand. Except for the case-hardened surfaces the rock is extremely friable, which made sample collection and coring difficult. Commonly the only recoverable portion of cores was the case-hardened surface. When cored, both silica and iron-oxide case-hardening frequently yields only buttons of the case-hardened surface (Figure 9).

In thin section, sand grains are typically sub-rounded to angular quartz (Figure 10). Grain size ranges from clay to very coarse, with most grains being fine to coarse. Quartz grains are undulose and highly fractured. Mafic minerals and feldspars are present in very small quantities and are frequently in a state of partial disintegration. Clay-, silica-, and iron-type cement have been identified by visual inspection of the thin sections. Clay and silica cement occur throughout the thin-sections, while iron oxide occurs only in some case-hardened surfaces. Clay cement occurs in all thin sections.

Typically, clay rims surround quartz grains and sometimes fills portions of the pore space near where grains meet. Locally, more pervasive clay cement fills pore spaces (Figure 11). Though difficult to identify in thin section, clay cement appears to be composed of smectite and kaolinite.

Silica cement is also present in all thin sections, though slightly less common than clay and much more difficult to observe without cathodo luminescence. This cement is difficult to distinguish from quartz grains, but can be detected where there are dust rims between the original grain and the overgrowths, or where there are fractures in the original grain that do not extend into the overgrowth (Figure 12). Silica overgrowths tend to have precipitated in pore spaces, but sometimes connect multiple grains, contributing to cementation of the rock. Silica overgrowths are sometimes found beneath clay and iron oxide cements, though it is more common where clay and iron oxide are absent. Though silica cement is present throughout the rock, it is slightly more common near the surface of silica case-hardened samples.

Silica cement was further analyzed using cathodo luminescence. Images using this method show the original quartz grains as shades of gray, while quartz overgrowths appear black (Figure 13). Original grain boundaries were traced using Esri ArcGIS and differentiated where silica overgrowths connected to other grains and contributed to cementation (Figure 14). Samples with goethite cement were excluded because the pervasive cement and quartz overgrowths both appear black using cathodo luminescence and could not be differentiated. Results from the four analyzed images ranged from 5.6-9.4% of the original grain boundaries are silica cemented, with an average of 7.9% (Table 4).

Differences in the rock structure were also observed in thin section. Four samples were identified with more tightly packed grains at the rock surface than the interior (Figure 15). In these samples, the surface of the rock contains abundant long and concavo-convex contacts with fewer point contacts than the interior of the rock. Smaller grain size also commonly occurs at the rock surface. In sample SIB1, pore spaces are filled with clay and very small angular quartz grains at the rock surface (Figure 16). An abundance of clay also occurs in the silica case-hardened portion of sample RI (Figure 17).

Iron oxide cement exists only in a few samples, and only near the surface of the rock. It is very pervasive, filling pore spaces almost entirely, and even filling micro-fractures in quartz grains (Figure 18). Iron oxide forms a distinct band on the fracture surface. Below the iron oxide band only meager iron oxide is observed. In some samples, iron oxide is less pervasive but still has a distinct front (Figure 19). Silica overgrowths are present beneath the iron oxide cement (Figure 18), but are more common where it is absent.

Measured porosity of cores ranges from 0.192 – 0.241 (mean = 0.219) (Table 5). Permeability with case-hardened surfaces intact ranged from 61 – 3583 mD (mean = 1370 mD). For most samples, permeability was also measured after the removal of the case-hardened surface. Permeability increased with the removal of the surface in all cases, with values ranging from 342 – 4834 mD (mean = 2333 mD).

Chemistry and Mineralogy

XRF results are similar across all samples, with a few exceptions (Table 6). All samples are mostly composed of silica (90.21 - 99.3%, mean = 96.97%). The next-most

abundant elements are aluminum (0.31 - 1.58%, mean = 0.86%) and iron (0.07 - 6.91%, mean = 0.71%). Other elements are present only in very small amounts (mean ≤ 0.11%).

Very little chemical variability occurs in silica-coated samples. The content of all analyzed elements is within 1 standard deviation of the mean in almost all cases. Iron coated samples contained more chemical variability. The prominent iron coating of sample ICS contains considerably more iron, phosphorous, uranium, lead, zinc, chromium, and vanadium than other samples (at least 3 standard deviations greater than the mean for each of these elements). Sample ICS only contained 90.21% silica, which is 3.5 standard deviations below the mean. The interior of the same sample was much closer to the average, with calcium and nickel 1-1.5 standard deviations below the mean, and all other elements less than 1 standard deviation about the mean.

Data collected in the field using pXRF is less accurate than lab XRF data. Weight percentages do not add up to 100% and are unreliable as absolute values. This data is useful, however, in comparing ratios of the elements detected. Many elements were analyzed, but the only strong correlation observed was between iron and titanium (Figure 20).

RockJock11 (Eberl, 2003) was used to obtain mineralogical data (Table 7). The most dominant mineral phase in all samples is quartz, ranging from 91-97% (mean = 94.5%), the remainder of the rock being composed of feldspars, kaolinite, smectite, and geothite. Because quartz is so abundant, other minerals are necessarily present only in small quantities and are less accurately detected using this method. For example, all samples returned values of ~2-4% feldspar. K and Ca levels from XRF analysis are too low to support much feldspar in the rock (means = 0.10% and 0.04%, respectively), nor is

it observed in large quantities in thin section. Additionally, clays can be poorly crystalized and may actually be present in larger quantities than indicated by RockJock11. The results for non-quartz minerals are better interpreted non-quantitatively, present as minor constituents.

As with the XRF analysis, XRD results generally do not vary much between the coating and interior of the rock. The exception again is sample ICS, in which the coating contains ~3% goethite, but the interior does not contain a detectible amount. This reflects the XRF results and indicates that iron-type case-hardening is composed of goethite. Other variations between the coating and interior of samples is within the range of error and not conclusive.

DISCUSSION

One of the most puzzling questions about the rock at Adršpach-Teplice is how such a friable sandstone can maintain vertical walls upwards of 60m in height. It has been suggested that the vertical walls are in part the result of a locked sand structure (Bruthans, in progress). A locked sand has undergone some diagenesis by pressure solution but has not undergone the thorough cementation and induration of a sandstone. The Adršpach-Teplice sandstone meets the five major characteristics for a locked sand as described by Dussealt and Morgenstern (1979):

i. A porosity less than the minimum attainable in the laboratory, which is 32.7(±3.7)% in the case of very well-sorted, fine grained clean sands and for medium- to coarse-grained sands
ii. A quartzose composition
iii. A diagenetic fabric and associated grain surface texture

iv. Generally older than Quaternary

v. Little or no true intergranular cement

The diagenetic fabric described in characteristic iii refers to dissolution at grain contacts where stresses are highest, and precipitation of overgrowths that typically form on areas of grains not in contact with other grains. The result is a conversion of point contacts to long and concavo-convex contacts with an overall reduction in porosity. The undulose, fractured nature of the quartz grains observed in thin section is consistent with the stresses due to burial that bring about pressure solution.

Studies by Dussealt and Morgenstern (1979) and Barton (1993) conclude that locked sands are desirable geotechnical materials and have high shear and tensile strength. These studies also mention that locked sands are moisture sensitive and can disintegrate readily when placed unsupported in water. This explains the difficulty experienced in coring the rock at Adršpach-Teplice using water as a coolant.

Silica Case-Hardening

It is clear that silica case-hardened surfaces, which compose the majority of rock faces at Adršpach-Teplice, are more strongly cemented than the interior of the rock. While silica cement is clearly a player in holding the rock together, it is not likely the only factor responsible for the increased strength of the surface 1-2mm. In thin section, silica overgrowths are visible throughout the observed portion of the rock (up to about 10 cm depth), with only a very minor increase in abundance near the surface. An increase of clay at the surface was observed in thin section for samples SIB1 and RI, which may contribute to case-hardening. However, this was not observed in other samples and thus cannot be a complete explanation for the presence of case-hardening.

XRF and XRD results show virtually no compositional or mineralogical variation between the surface and interior of silica case-hardened samples. This implies that the case-hardening is not the result of the introduction of new material, but rather the rearrangement of what is already present through physical or chemical means. As previously stated, the increase in abundance of quartz overgrowths at the rock surface is only minor and probably contributes little to case-hardening.

A reduction in porosity due to more tightly packed grains was observed in the case-hardened surfaces of samples 3, 5, ICS, and SIB1 in thin section (Figure 15). A reduction of grain size was also observed in the case-hardened surfaces of samples ICS and SIB1. These observations are consistent with deformation bands. A review of deformation bands in sandstone by Fossen et al. (2007) categorizes four types of deformation bands, two of which are observed in thin sections from Adršpach-Teplice: disaggregation bands and cataclastic bands. Disaggregation bands develop from shear motion producing grain rolling and grain boundary sliding (referred to as granular flow) which can result in a reduction in porosity and permeability. Where mechanical grain fracture is significant, cataclastic deformation bands form, resulting in grain-size reduction, angular grains, and an absence of pore space. These processes occur over small displacements, usually less than 3-4 cm. Samples 3 and 5 are consistent with disaggregation bands, while samples ICS and SIB1are consistent with cataclastic deformation bands.

Permeability was measured for both the surface and interior of three of the four samples with an observed decrease in porosity in the case-hardened surface due to grain packing (sample ICS was insufficient in length and was only measured with the case-

hardened surface intact). Each of these samples had lower permeability in the case-hardened surface than the interior of the rock. Of special note is sample SIB1, in which the interior of the rock had a permeability two orders of magnitude higher than the case-hardened surface. It is common for cataclastic deformation bands to reduce permeability two to three orders of magnitude (Fossen et al., 2007).

Silica case-hardening has been observed to form on young rock faces, including inscriptions as young as 30 years old and quarried faces only five years old. A study of a similar sandstone quarry by Bruthans et al. (2012b) found case-hardening to be fully developed in 6 years in favorable conditions, with an appearance and increase in strength similar to that seen at Adršpach-Teplice. This is probably due to a slight increase in silica precipitation due to evaporation at the surface, the introduction of biological material, and possibly deposition of atmospheric dust. Silica deposition and biological activity may go hand in hand; cyanobacteria have been observed to create local shifts in pH from as low as 3.4 to over 9.0, which is necessary for silica dissolution (Brehm et al., 2004).

Iron Oxide Case-Hardening

Unlike silica cement, which occurs throughout the rock, iron oxide was observed only up to one centimeter deep in the rock. The primary chemical difference observed in XRF data was in increase in iron in the case-hardened surface. XRD analysis confirms that this iron is present as the mineral goethite.

The presence of goethite only at the surface of the rock suggests that water with Fe^{2+} as a dissolved constituent reached an oxidation front where the iron was precipitated as goethite. This makes sense in the context of the field area. Above the exposed faces is

abundant organic material, which can create the reducing environment necessary to dissolve Fe^{2+}. Upon reaching the rock faces, atmospheric oxygen is encountered and conditions shift from reducing to oxidizing. The tendency of iron to precipitate in bedding planes suggests that Fe^{2+} bearing water is transported through the rock within high-porosity bedding planes and then trickles over the face of the rock. As indicated in XRF analysis, there is very little iron present in the interior of the rock, so iron probably originated from an external source. Likely candidates include the previously overlying material that has since eroded away or atmospheric dust.

Where iron case-hardening is observed in the field, it is typically not extensive and shows evidence of weathering. Weathering is also apparent in thin section, where some samples lack the pervasiveness of this case-hardening, but still have a distinct front beneath which no goethite is present (Figure 19). Additionally, iron oxide case-hardening was not observed on inscriptions in the rock or on quarried surfaces. This may indicate that iron oxide is not presently being precipitated.

Results from pXRF measurements in the field indicate that iron oxide case-hardening has an increased amount of titanium (Figure 20). It is still unclear why relatively immobile titanium would be present in conjunction with iron oxide, and further study should be done before conclusions are drawn.

Timing of Events

There are three major characteristics of the sandstone at Adršpach-Teplice that result in the strength of fracture faces and allow for the formation and preservation of vertical walls: the structure of the rock, the presence of iron case-hardening, and the

presence of silica case-hardening. The processes responsible for these features can be ordered chronologically based on observations in thin section and in the field.

Locked sand structure and deformation bands are present beneath both types of case-hardening, indicating that structural changes were the first to occur. The fact that disaggregation bands in the sandstone are well preserved indicates that they must have occurred relatively early in diagenesis. Disaggregation bands form through the rolling and shifting of sand grains, a process that can break up cement to create zones of weakness despite a decrease in porosity. The fact that disaggregation bands observed at Adršpach-Teplice are stronger than other portions of the rock indicates that cementation must have occurred in large part after the formation of fractures and deformation bands.

Barton (1993) describes the typical processes responsible for the formation of locked sands, which appear to be consistent with what is observed in the rock at Adršpach-Teplice. Several processes occur simultaneously. Pressure solution of quartz at grain contacts converts those contacts from tangential to long to concavo-convex and porosity is reduced. Silica dissolved during pressure solution can precipitate as overgrowths on quartz grains, primarily in pore spaces, and can contribute to cementation. While this occurs, feldspars and heavy minerals decompose and are converted into clays which are deposited as passive cements. These processes require the material to have been buried deeply. However, the absence of sutured grain contacts indicates only moderate depth of burial. This likely occurred very slowly sometime during the roughly 90 million years between deposition and surface exposure.

Of the two case-hardening types, it appears the iron-oxide was first to be deposited. Though there are silica overgrowths where there is iron oxide cement, their

abundance on the rock face is similar to that in the interior of the rock and does not have the slight increase near the surface seen in silica case-hardened surfaces. Furthermore, iron oxide always appears to be in some stage of erosion and is not observed on young rock exposures. Precipitation of goethite requires oxidizing conditions, so this must have occurred when the rock was exposed or in the very shallow subsurface in the presence of atmospheric oxygen.

Finally, silica case-hardening formed on the rock surface and continues to form currently. This case-hardening depends on evaporative and biological processes and must have occurred after the exhumation of the rock. Its ubiquity and rapid formation create a protective coating on virtually all of the rock at Adršpach-Teplice. Silica case-hardening can be quickly deposited on surfaces where erosion has recently occurred, and is thus essentially a self-repairing material.

CONCLUSIONS

1. The locked sand structure (created by pressure solution of quartz) of the rock at Adršpach-Teplice is important in the formation and maintenance of features seen in the rock city. This structure is clearly observed in thin section and gives the rock the strength to maintain vertical faces despite poor cementation and friability.
2. Disaggregation and cataclastic bands are present parallel to and at the surface of some fractures. These reduce porosity and are probably in part responsible for the increased strength in case-hardened surfaces.
3. Silica case-hardening is ubiquitous in Adršpach-Teplice and can form as quickly as within 5 years. The case-hardened surface includes a slight increase in silica overgrowth abundance and sometimes clay. Clay either originates from the interior

of the rock and is trapped in the reduced porosity of deformation bands or originates from atmospheric dust. Biological material is also present and may aid in the dissolution of quartz necessary to form silica overgrowths.

4. Iron case-hardening is less common and probably less important in preserving fracture faces. It is composed of goethite and is not found in the interior of the rock. It is commonly precipitated on bedding surfaces, indicating that Fe^{2+} bearing water probably flows along bedding surfaces. Upon reaching the oxidizing conditions at fractures exposed to the atmosphere, goethite is precipitated. The interior of the rock contains very little iron, so the source for iron case-hardening is probably external.
5. The order of events responsible for forming case-hardened surfaces is:
    a. Deposition and relatively shallow burying of deltaic sand.
    b. Formation of fractures and deformation bands due to regional stresses. Regional fractures are oriented NW-SE, with conjugate fractures oriented NE-SW
    c. Formation of locked sand structure over a long time period, possibly tens of millions of years. This includes:
        i. pressure solution of quartz converting contacts from tangential to long and concavo-convex
        ii. precipitation of silica overgrowths
        iii. and breakdown of feldspars and heavy minerals into clays, which are distributed as passive cements
    d. Exhumation of sandstone
    e. Iron oxide is deposited in oxidizing conditions at or near the vadose zone

f. Silica case-hardening forms on rock surfaces in the vadose zone where evaporation is a factor. Silica case-hardening continues to develop modernly.

REFERENCES

Adamovic, J., Mikulas, R., Schweigstillova, J., and Boehmova, V., 2011, Porosity Changes Induced by Salt Weathering of Sandstones, Bohemian Cretaceous Basin, Czech Republic: Acta Geodynamica Et Geomaterialia, v. 8, p. 29-45.

Barnet, I, and Burda J., 1997, Vysvetlivky ke geologickym mapam (explanatory notes to geology maps), 1:50000. Sheets 04-31, 32, 33, 34.

Barton, M., 1993, Cohesive sands: the natural transition from sands to sandstones: Geotechnical Engineering of Hard Soils-Soft Rocks, Balkema, Rotterdam, v. 1, p. 367-374.

Brehm, U., Gorbushina, A., and Mottershead, D., 2005, The role of microorganisms and biofilms in the breakdown and dissolution of quartz and glass: Palaeogeography Palaeoclimatology Palaeoecology, v. 219, p. 117-129, doi: 10.1016/j.palaeo.2004.10.017.

Bruthans J., Churackova Z., Jenc P., Schweigstillova J., 2009, Age and origin of secondary carbonates from several caves in the Bohemian Paradise (in Czech): Czech Geological Survey, Geoscience Research Reports for 2008, p. 54-58.

Bruthans, J., Schweigstillova, J., Jenc, P., Churackova, Z., and Bezdicka, P., 2012a, C-14 and U-Series Dating of Speleothems in the Bohemian Paradise (Czech Republic): Retreat Rates of Sandstone Cave Walls and Implications for Cave Origin: Acta Geodynamica Et Geomaterialia, v. 9, p. 93-108.

Bruthans, J., Svetlik, D., Soukup, J., Schweigstillova, J., Valek, J., Sedlackova, M., and Mayo, A.L., 2012b, Fast evolving conduits in clay-bonded sandstone: Characterization, erosion processes and significance for the origin of sandstone landforms: Geomorphology, , doi: 10.1016/j.geomorph.2012.07.028.

Carter, C.L., and Anderson, R.S., 2006, Fluvial erosion of physically modeled abrasion-dominated slot canyons: Geomorphology, v. 81, p. 89-113, doi: 10.1016/j.geomorph.2006.04.006.

Cilek, V., and Zak, K., 2007, Late glacial and Holocene sedimentation under sandstone rock shelters of Northern Bohemia (Czech Republic) *in* Geodiversity of sandstone landscapes Hartel, Cilek, Herben, Jackson and Williams ed: Academa p. 133-138.

Conca, J.L., and Rossman, G.R., 1982, Case hardening of sandstone: Geology (Boulder), v. 10, p. 520-523.

Dusseault, M.B., and Morgenstern, N.R., 1979, Locked sands: The Quarterly Journal of Engineering Geology, v. 12, p. 117-131.

Eberl, D. D., 2003, User's guide to RockJock – A program for determining quantitative mineralogy from powder X-ray diffraction data, revised November 30, 2009, USGS Open File Report 03-78, 48 p.

Fossen, H., Schultz, R.A., Shipton, Z.K., and Mair, K., 2007, Deformation bands in sandstone: a review: Journal of the Geological Society, v. 164, p. 755-769, doi: 10.1144/0016-76492006-036.
Garvie, L.A.J., Burt, D.M., and Buseck, P.R., 2008, Nanometer-scale complexity, growth, and diagenesis in desert varnish: Geology, v. 36, p. 215-218, doi: 10.1130/G24409A.1.
Kunes, P., Pokorny, P., and Jankovska, V., 2007, Post-glacial vegetation development in sandstone areas of the Czech Republic in Härtel H., Cílek V., Herben T. Jackson A. and Williams R. eds: Academia p. 244-257
Laurin, J., and Ulicny, D., 2004, Controls on a shallow-water hemipelagic carbonate system adjacent to a siliciclastic margin: Example from late turonian of Central Europe: Journal of Sedimentary Research, v. 74, p. 697-717, doi: 10.1306/020904740697.
McFarlane, M.J., 1992, Groundwater movement and water chemistry associated with weathering profiles of the African surface in part of Malawi: Geological Society of London, Special Publications, v. 66, p. 101-129.
Novak, J., Sadlo, J., and Svobodova-Svitavska, H., 2012, Unusual vegetation stability in a lowland pine forest area (Doksy region, Czech Republic): Holocene, v. 22, p. 947-955, doi: 10.1177/0959683611434219.
Perry, R., Lynne, B., Sephton, M., Kolb, V., Perry, C., and Staley, J., 2006, Baking black opal in the desert sun: The importance of silica in desert varnish: Geology, v. 34, p. 537-540, doi: 10.1130/G22352.1.
Pokorny, P., 2002, A high-resolution record of Late-Glacial and Early-Holocene climatic and environmental change in the Czech Republic: Quaternary International, v. 91, p. 101-122, doi: 10.1016/S1040-6182(01)00105-7.
Potter, R., and Rossman, G., 1977, Desert Varnish - Importance of Clay-Minerals: Science, v. 196, p. 1446-1448, doi: 10.1126/science.196.4297.1446.
Prikryl, R., Melounova, L., Varilova, Z., and Weishauptova, Z., 2007, Spatial relationships of salt distribution and related physical changes of underlying rocks on naturally weathered sandstone exposures (Bohemian Switzerland National Park, Czech Republic): Environmental Geology, v. 52, p. 283-294, doi: 10.1007/s00254-006-0589-2.
Rogers, C.M., and Engelder, T., 2004, The feedback between joint-zone development and downward erosion of regularly spaced canyons in the Navajo Sandstone, Zion National Park, Utah: Geological Society Special Publications, v. 231, p. 49-71.
Stejskal, V., 2005, Morphostructural analysis of landforms in Polická vrchovina (in Czech), Czech Association of Geomorphologists, Accessible online: http://www.kge.zcu.cz/geomorf/sbornik/sbornik_05/stejskal.pdf (9/2012)
Svoboda, M., 1970, The hydrological budget and computation of ground-water components of river discharge in the north-west part of Police representative basin in Czechoslovakia: Journal of Hydrology, v. 9, n. 2, p. 252-280.
Thiagarajan, N., and Lee, C., 2004, Trace-element evidence for the origin of desert varnish by direct aqueous atmospheric deposition: Earth and Planetary Science Letters, v. 224, p. 131-141, doi: 10.1016/j.espl.2004.04.038.

Ulicny, D., 2001, Depositional systems and sequence stratigraphy of coarse-grained deltas in a shallow-marine, strike-slip setting: the Bohemian Cretaceous Basin, Czech Republic: Sedimentology, v. 48, p. 599-628, doi: 10.1046/j.1365-3091.2001.00381.x.
Ulicny, D., Laurin, J., and Cech, S., 2009, Controls on clastic sequence geometries in a shallow-marine, transtensional basin: the Bohemian Cretaceous Basin, Czech Republic: Sedimentology, v. 56, p. 1077-U41, doi: 10.1111/j.1365-3091.2008.01021.x.
Varilova, Z., 2007, Occurrences of Fe-mineralization in sandstones of Bohemian Switzerland National Park (Czech Republic): Academia of Sciences of the Czech Republic, Praha, Czech Republic (CZE), .
Viles, H., and Goudie, A., 2004, Biofilms and case hardening on sandstones from Al-Quwayra, Jordan: Earth Surface Processes and Landforms, v. 29, p. 1473-1485, doi: 10.1002/esp.1134.

FIGURES

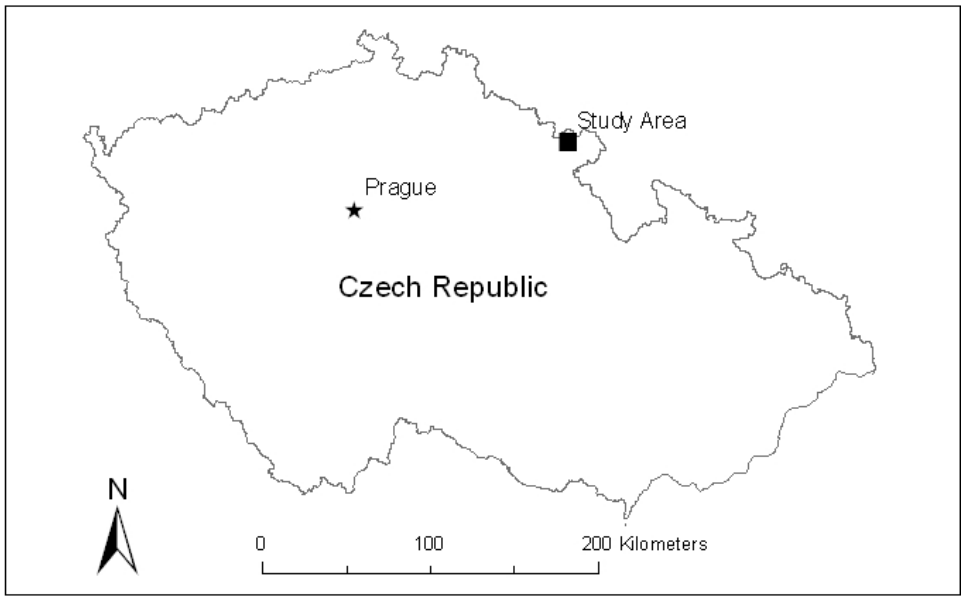

Figure 1. Map of the Czech Republic showing the study area.

Figure 2. Non-orthographic aerial photograph of Rock Island. North is approximately at the top of the photo. Note the dominant fracture set running roughly NW-SE and conjugate fractures roughly NE-SW (see Figure 4).

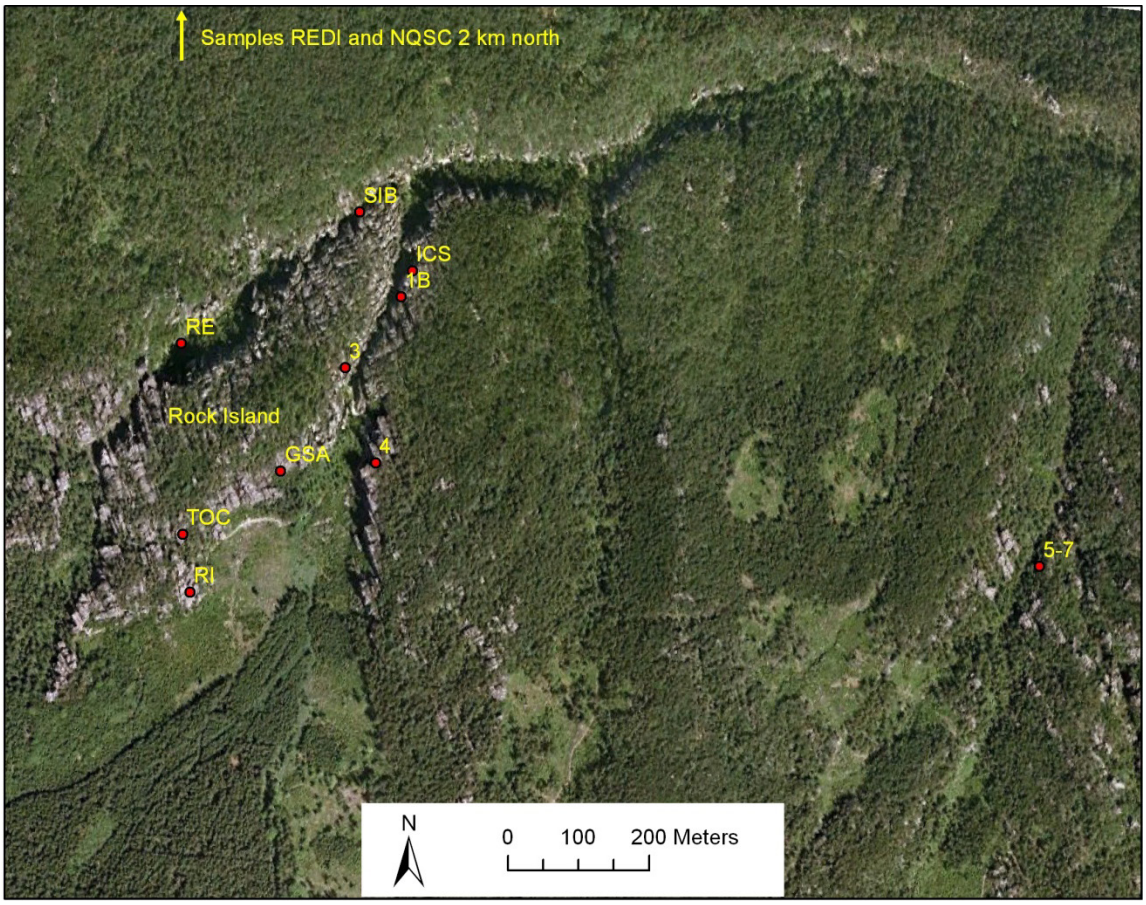

Figure 3. Sample location map. For information on individual samples, see Table 1.

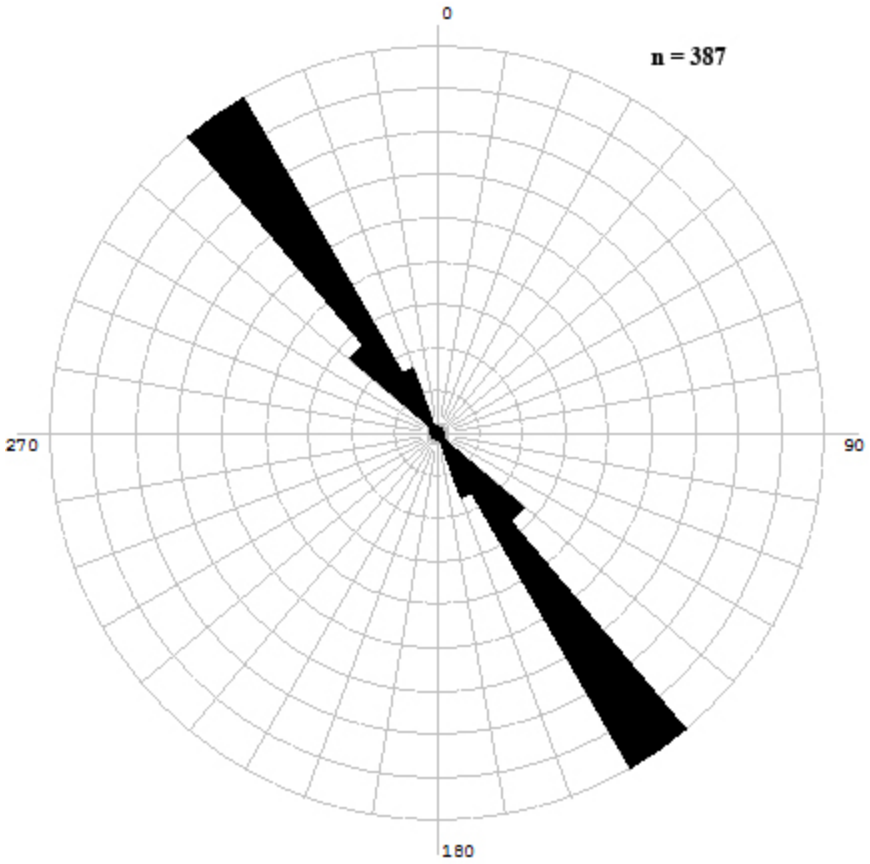

Figure 4. Rose diagram showing orientation of regional fractures in Rock Island. Conjugate fractures were not measured due to inaccessibility, but are oriented approximately 90° from regional fractures.

Figure 5. Open fracture in Rock Island. Fractures are sub-vertical even when exposed.

Figure 6. Slot canyon in Rock Island. Fracture faces are open in the slot canyon and closed beyond the back of the canyon. Sapping breaks material between fractures into rectangular blocks.

Figure 7. Closed fractures in Rock Island.

Figure 8. Iron oxide case-hardening. The patchy, partially eroded appearance is common on open fractures. Note the two horizontal bands of iron oxide formed along bedding planes.

Figure 9. Core buttons (2.54 cm diameter) with case-hardened surface. Left and center samples are silica case-hardened, right sample is iron case-hardened.

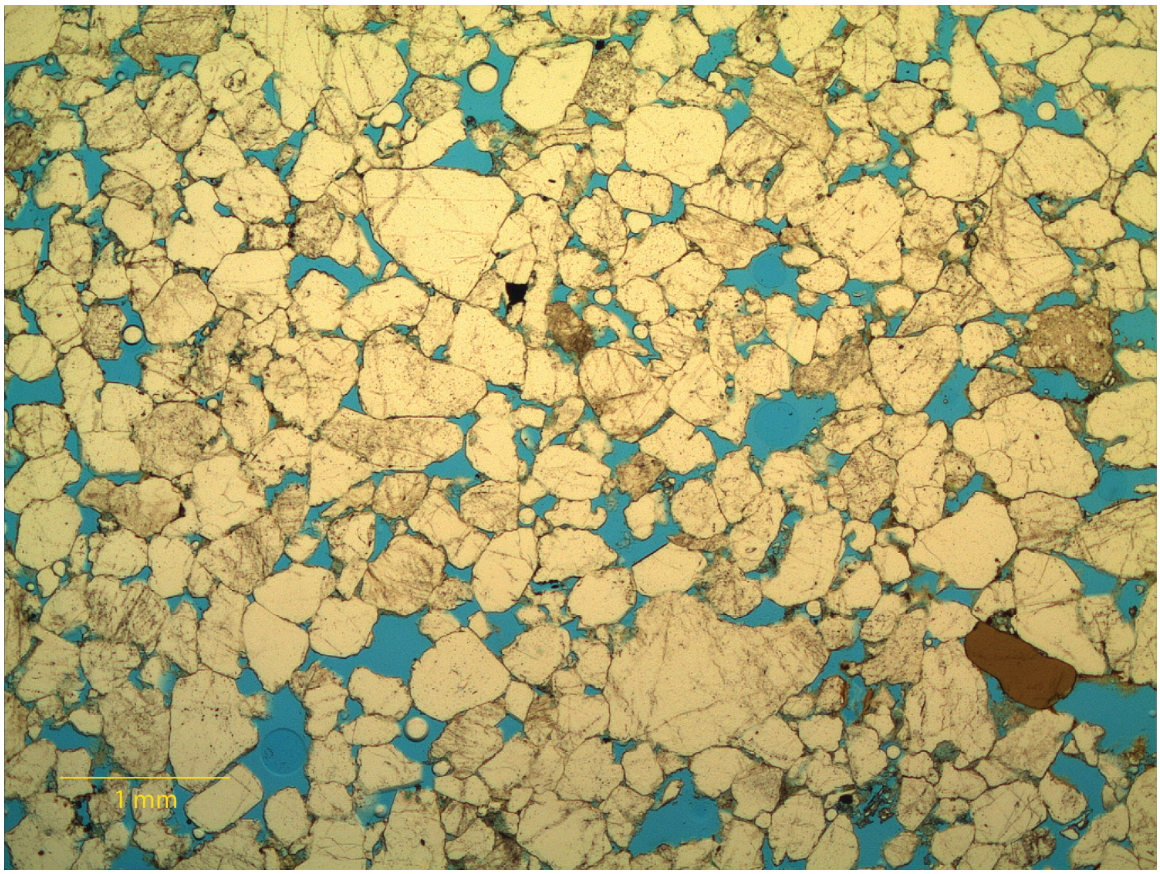

Figure 10. Interior of rock. Grains are typically sub-rounded to angular quartz. Grains are highly fractured. Blue represents porosity.

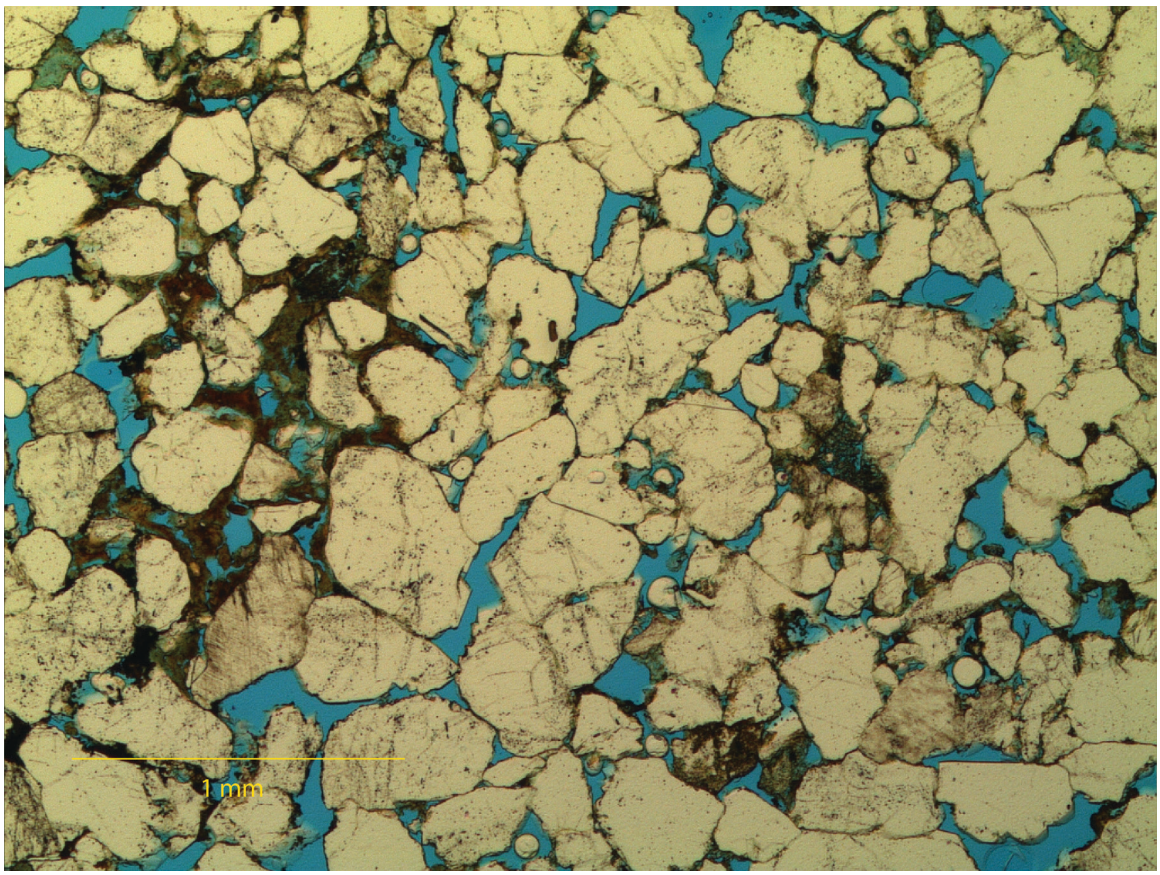

Figure 11. Clay cement in thin section. Clay is most commonly seen as very thin rims around grains. In a few cases, more pervasive clay cement fills pore spaces, as seen on the left side of image. Blue represents porosity.

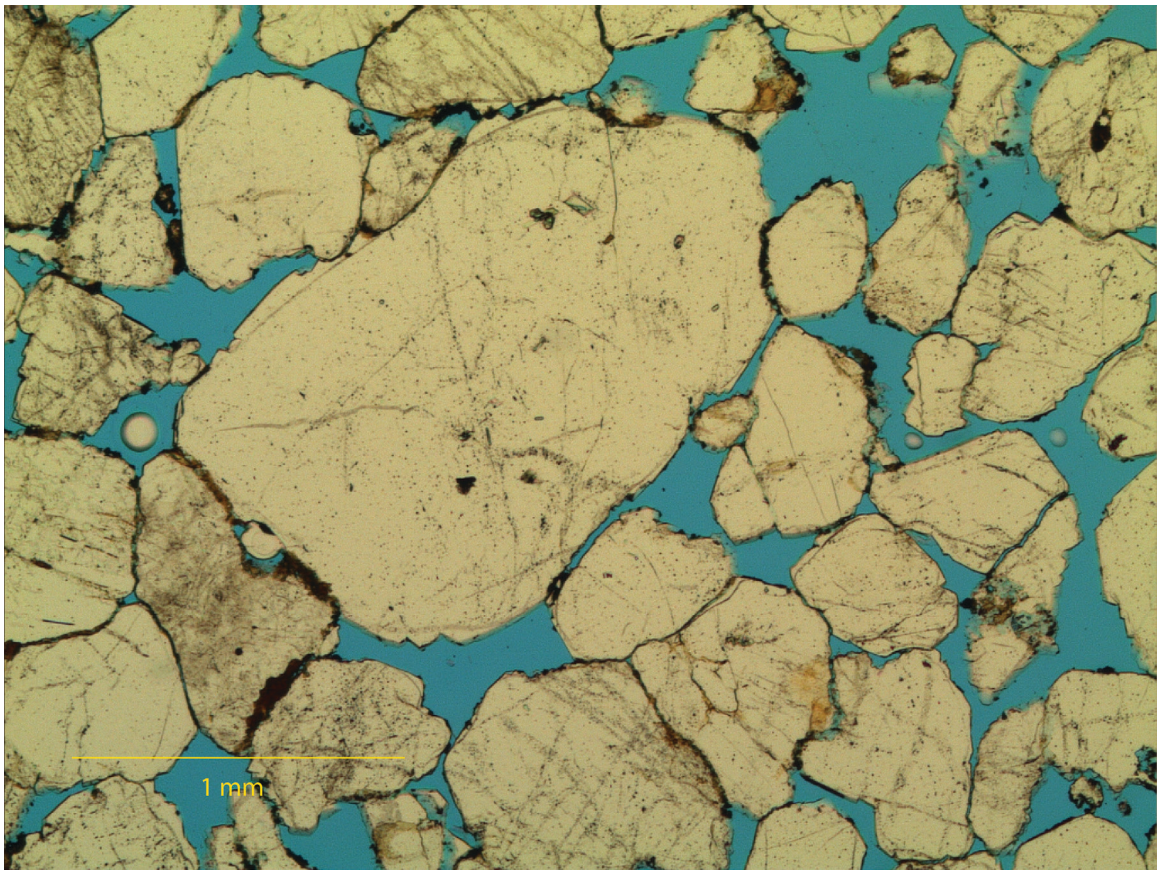

Figure 12. Silica overgrowths in thin section TOC, taken from the top of a sandstone pillar. Most grains in this image have silica overgrowths, but are most easily observed in the large grain in the center. Very thin dust rims can be observed between original grain and overgrowths. In the upper left portion of the center grain, silica overgrowths are clearly contributing to cementation. Blue represents porosity.

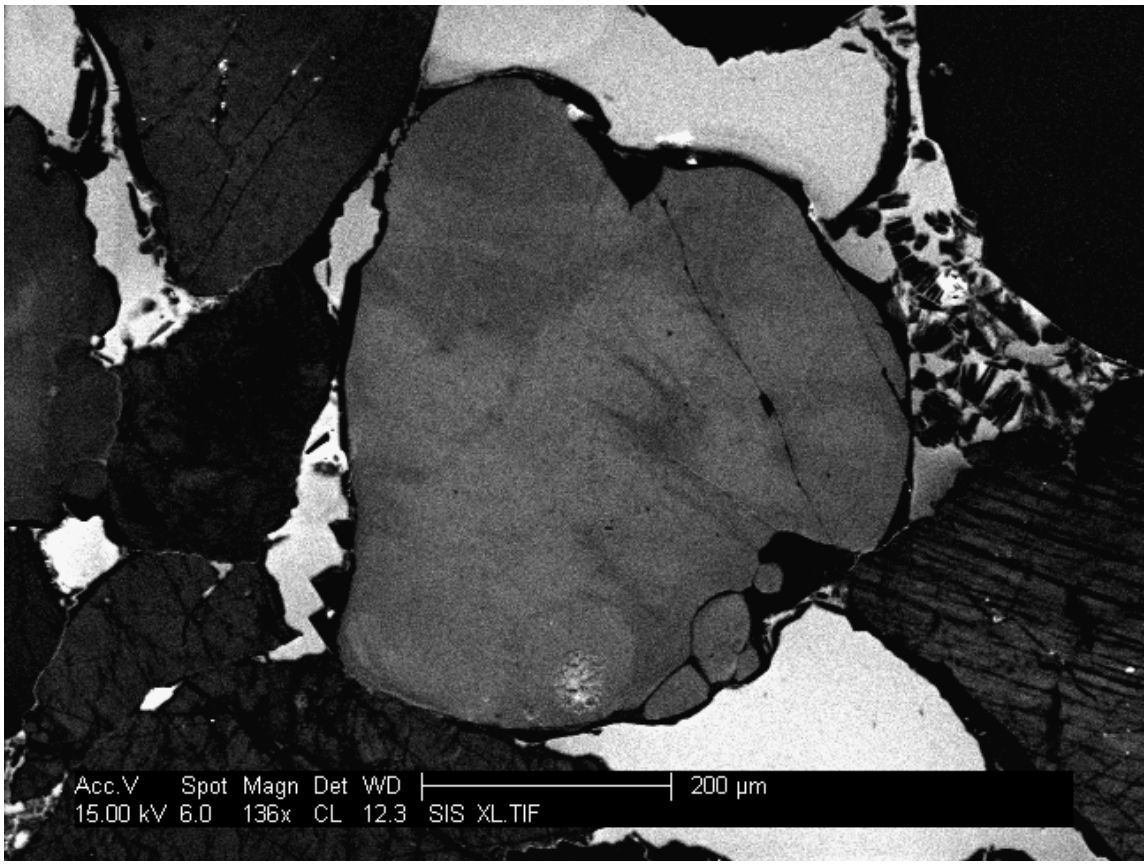

Figure 13. Silica overgrowths using cathodo luminescence. Quartz grains appear in shades of gray, while overgrowths appear black.

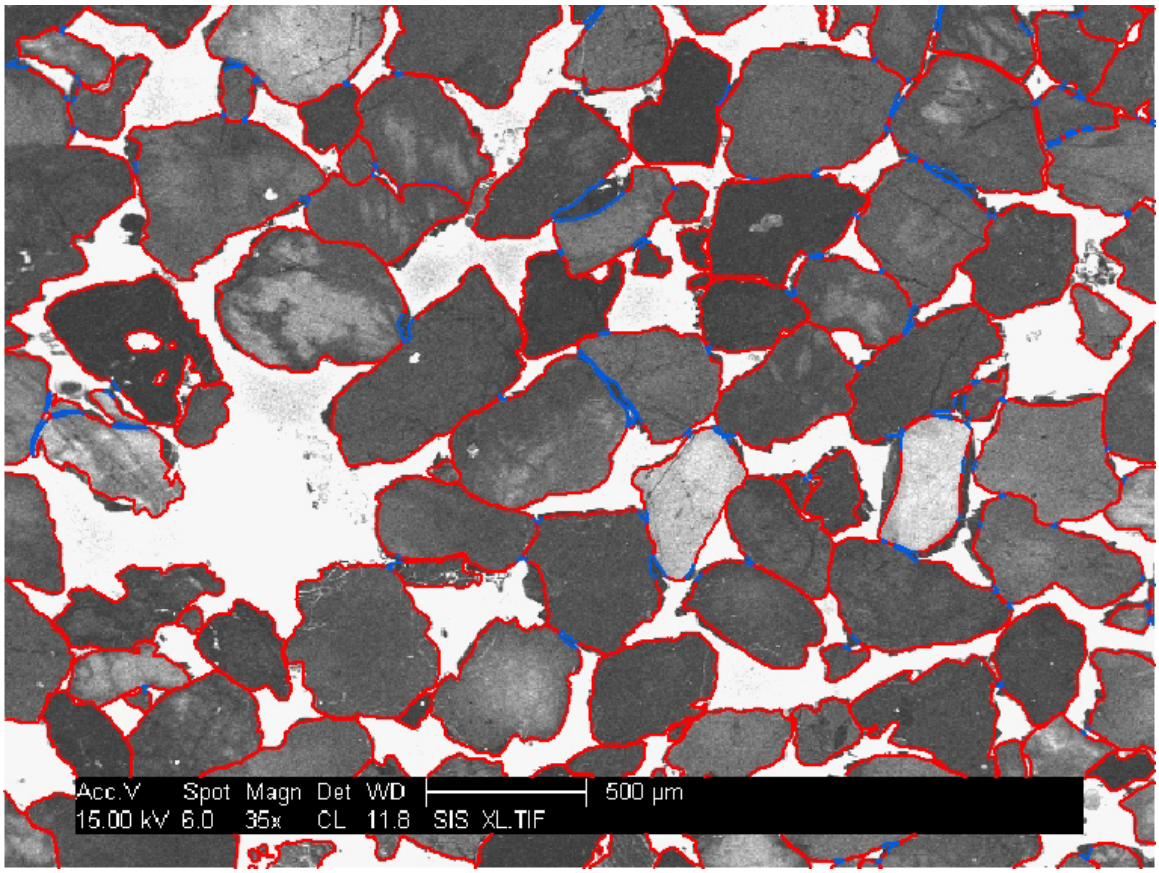

Figure 14. ArcGIS mapping of grain boundaries to quantify silica cementation. Blue represents where the original grain boundary is cemented due to silica overgrowths. Red represents where silica overgrowths are not present or do not contribute to cementation. In this image, 9.0% of grain boundaries are silica cemented.

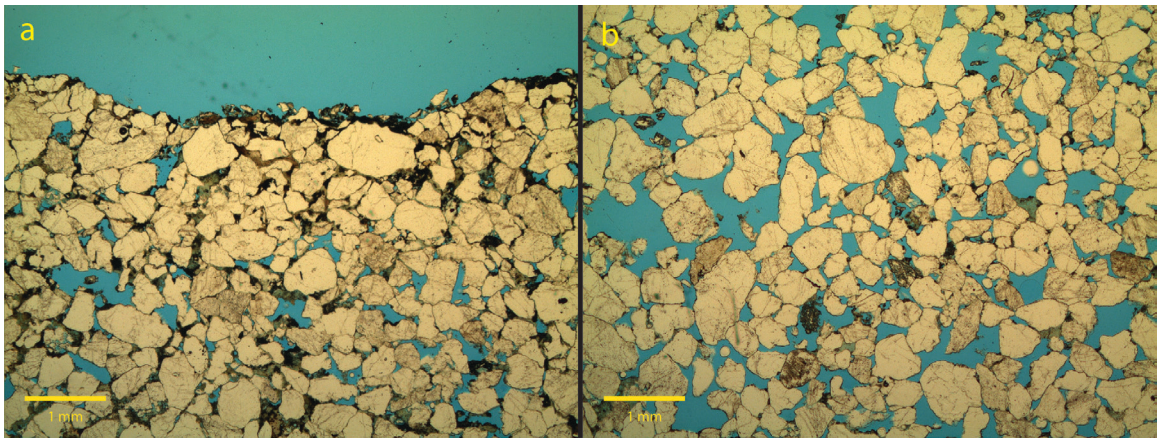

Figure 15. Thin sections of sample 5, showing (a) tight grain packing at the case-hardened surface and (b) looser grain structure with higher porosity in the interior of the rock.

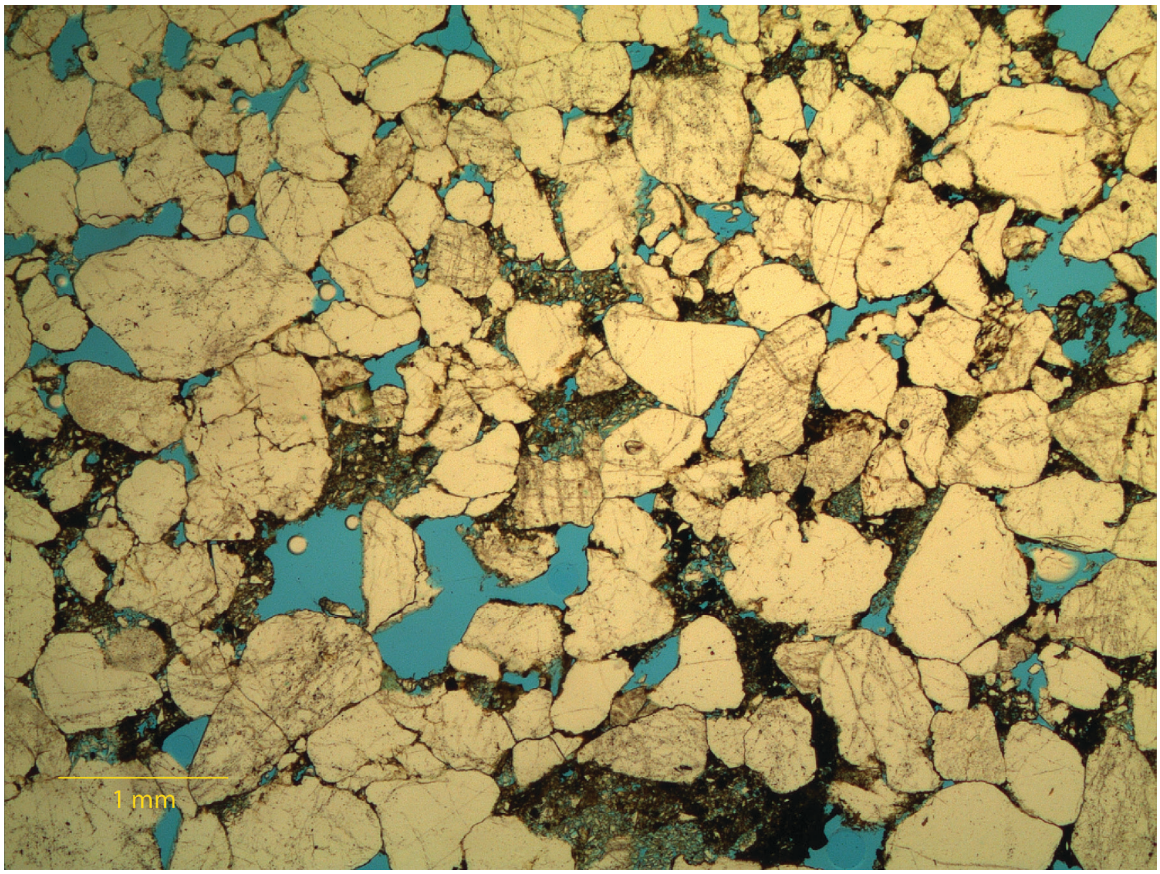

Figure 16. Thin section SIB1-C which cuts through case-hardened surface. Some pore spaces are filled with clay and very angular, very small quartz grains.

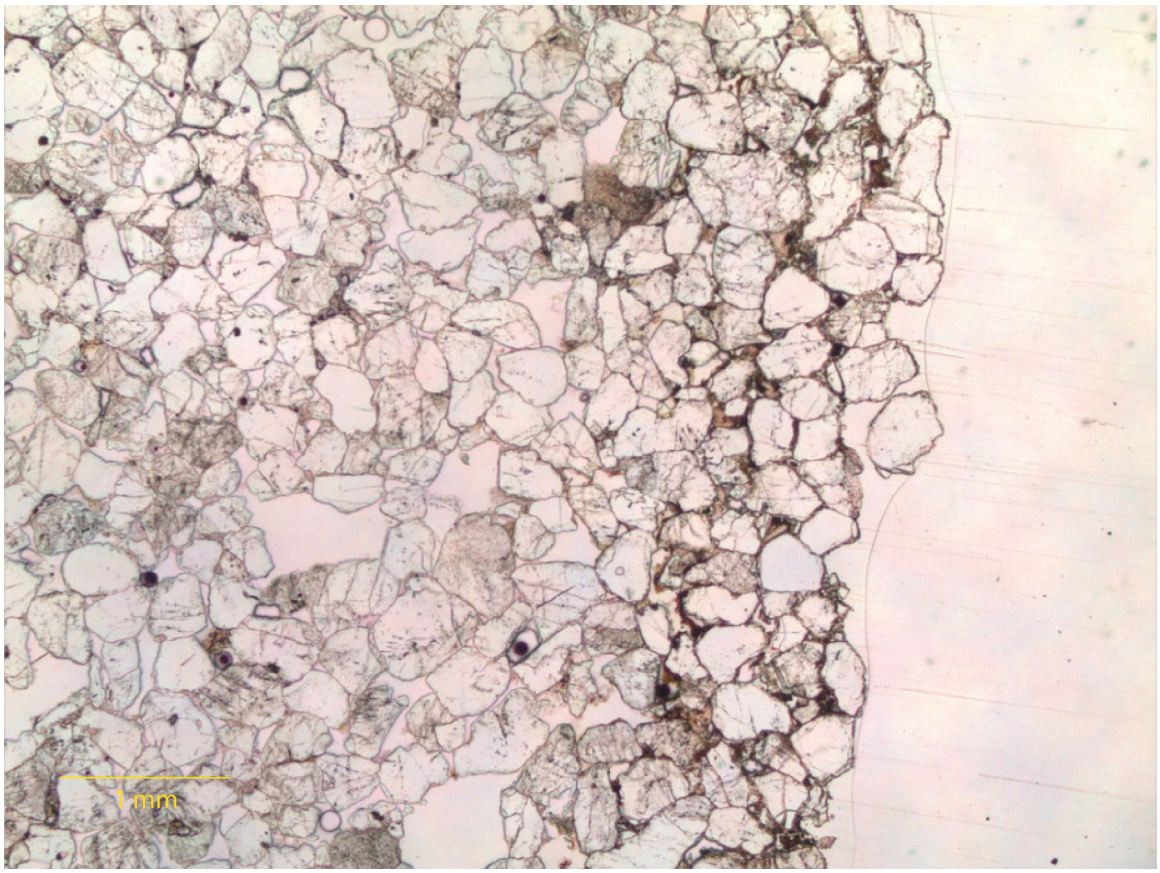

Figure 17. Thin section from sample RI showing an increased abundance of clay at the case-hardened surface (right side of image).

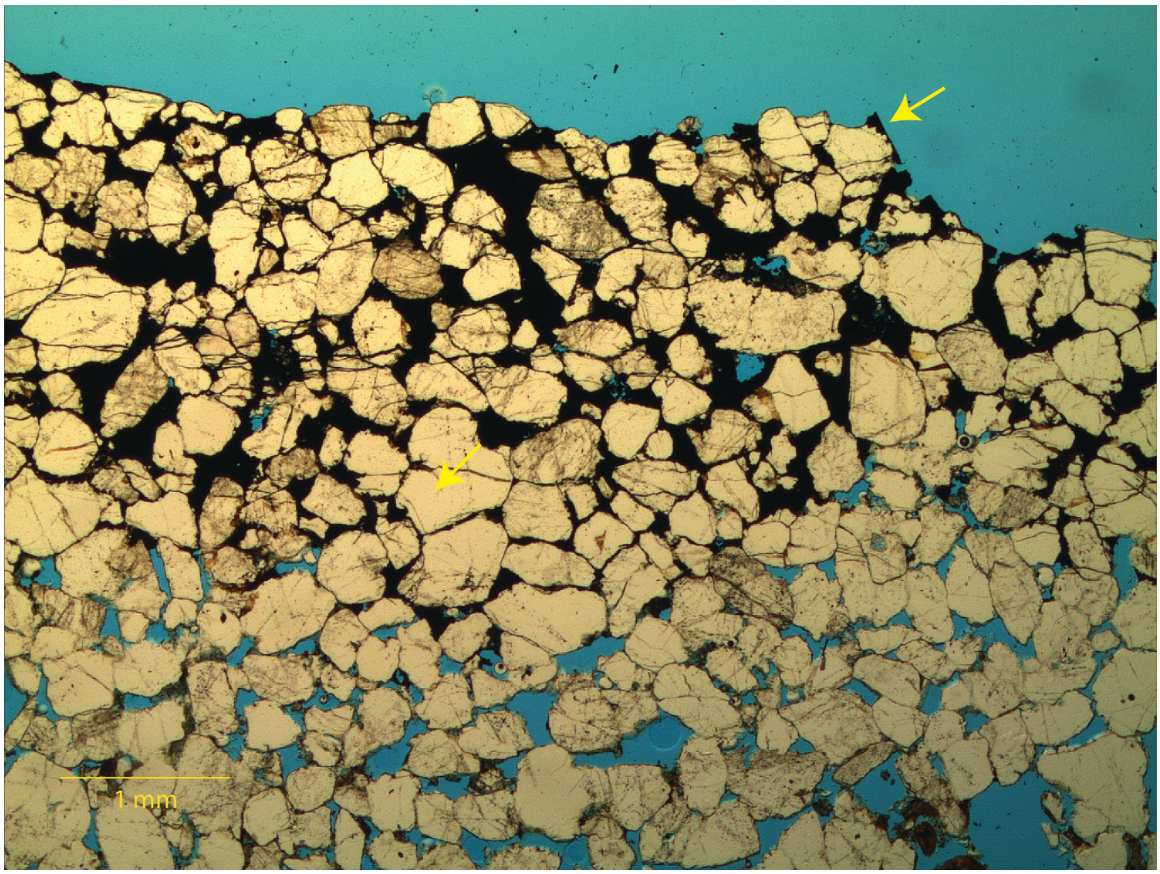

Figure 18. Iron case-hardening in thin section SIB5-C. Iron oxide exists only ~3mm deep in this sample. It is very pervasive, filling pore spaces and microfractures in quartz grains. Arrows indicate examples of grains with clearly visible silica overgrowths beneath iron oxide cement.

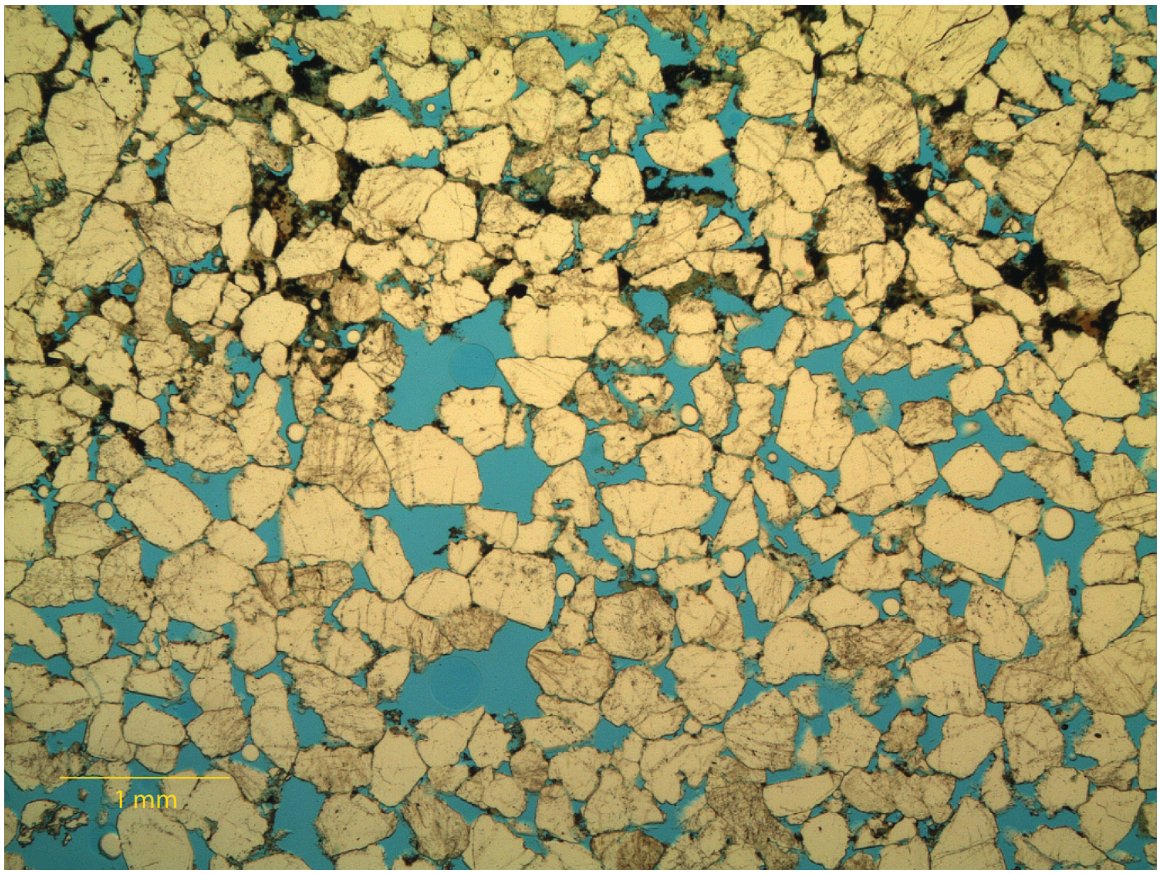

Figure 19. Less pervasive iron oxide case-hardening. Iron oxide fills only some pore spaces along with clay. There is a distinct boundary between where iron oxide is present and where it is not.

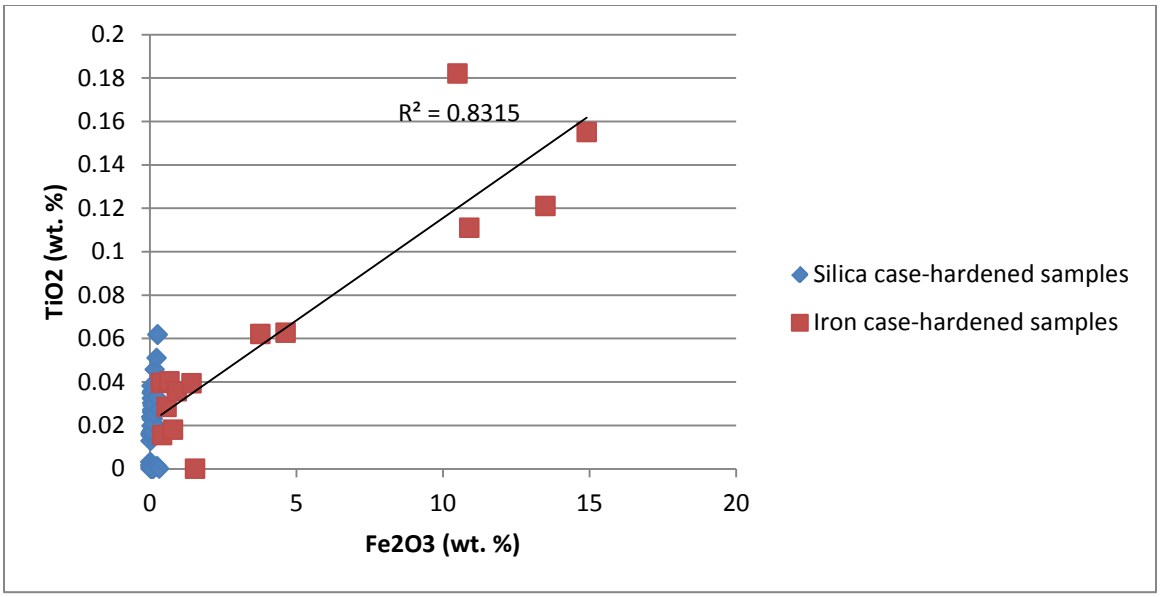

Figure 20. Correlation between iron and titanium in pXRF data.

TABLES

Table 1. Sample identification

Sample ID	Coating Type	Description
1B	Silica	Large sample recovered from Rock Island. Very friable. 2 cores were attempted in the lab, but were unsuccessful.
3	Silica	Large sample recovered from Rock Island. 4 cores taken in the lab.
4	Silica	Large sample recovered from Rock Island. 4 cores taken in the lab.
5	Iron	Large sample recovered from cave. Small amount of iron visible in coating. 1 core taken in the lab.
6	Silica	Large sample recovered from cave. Very friable. 2 cores were attempted in the lab, but were unsuccessful.
7	Iron	Large sample recovered from cave. Iron visible in coating. 3 cores taken in the lab.
SIB	Silica/Iron	Samples recovered from slot canyon known as Siberia in Rock Island. Cores 1-3 in silica coating, cores 4-6 in iron coating. Only cores 1 and 5 were sufficiently intact for porosity and permeability testing. Hand sample of silica coated rock collected for XRF analysis.
RI	Silica	Samples recovered from slot canyon in Rock Island. 7 cores attempted, only 1 recovered, but not sufficiently intact for porosity and permeability tests. Was used for XRF analysis. 3 coring attempts only surface coating remained intact (~1 cm). 3 coring attempts disintegrated completely.
REDI	Silica	Coring attempted in slot canyon known as Red Indian at the north end of the park. 2 cores attempted, only surface coating recovered (~1 cm)
NQSC	Silica/Iron	Coring and hand sample collection near a quarry at the north end of the park. 5 cores attempted in silica-coated rock, 4 disintegrated completely, 1 recovered only surface coating (~1 cm). 2 cores successfully recovered in iron-coated rock (~7 cm each). 2 hand samples of iron coating collected.
TOC	Silica	Sample collected from the top of a rock column in Rock Island. 1 core recovered in the lab.
RE	Silica	Large boulder near Rock Island. 6 cores attempted, but only surface coating was recovered (~1 cm).
GSA	Silica	Large sample recovered from Rock Island.
ICS	Iron	Sample collected from slot canyon near Rock Island almost entirely coated in iron. 1 core recovered in the lab.

Table 2. Summary of coring

	Cores attempted	Cores recovered, >3 cm, not usable	Cores recovered, >3 cm, usable	Buttons recovered (<3 cm)	Failed Cores
Field Coring, 2010	16	3	0	6	7
Field Coring, 2011	16	4	2	6	4
Lab Coring (Liquid Nitrogen Coolant)	18	0	13	1	4
Total	50	7	15	13	15

Table 3. Thin section sample identification

Sample ID	Source	Coating or Interior	Orientation Relative to Coating	Comments
1B-C	Core	Si Coating	Perpendicular	
3A-C	Core	Si Coating	Perpendicular	Polished, analyzed in ArcGIS
3A-I	Core	Interior	Perpendicular	
3D-C	Core	Si Coating	Parallel	
4A-C	Core	Si Coating	Parallel	
4A-I	Core	Interior	Perpendicular	
4B-C	Core	Si Coating	Perpendicular	
5-C	Core	Fe Coating	Perpendicular	
5-I	Core	Interior	Perpendicular	Polished, analyzed in ArcGIS
7A-C	Core	Fe Coating	Parallel	
7B-C	Core	Fe Coating	Perpendicular	
7B-I	Core	Interior	Perpendicular	
ICS-C	Whole Rock Sample	Fe Coating	Perpendicular	
RE-C	Whole Rock Sample	Si Coating	Perpendicular	
SIB 1-C	Core	Si Coating	Parallel	
SIB 1-I	Core	Interior	Perpendicular	
SIB 5-C	Core	Fe Coating	Perpendicular	Polished, analyzed in ArcGIS
SIB 5-I	Core	Interior	Perpendicular	
TOC-C	Whole Rock Sample	Si Coating	Perpendicular	
RI	Core	Si Coating	Perpendicular	Polished, analyzed in ArcGIS
NQSC-1	Core	Fe Coating	Perpendicular	Polished
NQSC-2	Whole Rock Sample	Fe Coating	Perpendicular	Polished

Table 4. Grain boundary mapping results

Sample ID	Percent Silica Cementation
3	7.4
5	9.4
RI	5.6
SIB	9.0

Table 5. Porosity and permeability results

Sample ID	Porosity	Permeability With Coating (mD)	Permeability Without Coating (mD)
3a	0.204	3460	3837
3b	0.238	2877	3947
3c	0.215	3583	4180
3d	0.241	3297	4403
4a	0.198	633	1192
4b	0.192	1100	1392
4c	0.197	463	1094
5	0.253	521	1138
7a	0.229	393	509
7b	0.231	798	853
7c	0.218	297	342
SIB 1	0.227	61	2733
SIB 5	0.201	327	2078
ICS1	0.227	-	2460
TOC	0.208	-	4834

Table 6. XRF Results

Sample ID	SiO2 mass%	Fe2O3 mass%	Al2O3 mass%	K2O mass%	TiO2 mass%	CaO mass%	P2O5 mass%	MgO mass%	Nb ppm	Zr ppm	Y ppm	Sr ppm	U ppm	Rb ppm	Th ppm	Pb ppm	Ga ppm	Zn ppm	Cu ppm	Ni ppm	Cr ppm	V ppm	Ba ppm	Sc ppm	LOI mass%	TOTAL mass%
1B																										
Coating	97.12	0.36	1.16	0.17	0.08	0.06	0.03	0.09	0.9	35	1.6	8.2	0	7.9	0.9	4.2	5.6	3.9	2.4	9.2	9.7	13.6	24.9	0	0.57	99.65
Interior	96.98	0.34	1.14	0.16	0.09	0.07	0.02	0.27	0.9	33.8	1.9	8.3	1.4	7.1	1.2	3.3	5.3	3.3	1.7	9.7	5.6	9.9	9	0	0.40	99.48
3																										
Coating	96.13	0.2	0.68	0.07	0.09	0.09	0.02	0.32	1.4	33.3	1.1	6.5	1	3.6	1.4	2.4	2.6	0.1	0.1	17.4	5	7.2	0	0	0.79	98.40
Interior	96.9	0.19	0.68	0.07	0.08	0.09	0.02	0.14	0.8	31.6	1	6.1	0	3.8	1.4	3.5	4.9	1.8	1.2	8.7	3.9	9.2	0	0	0.41	98.59
4																										
Coating	97.99	0.15	1.01	0.08	0.08	0.06	0.02	0.07	1.1	39.8	1.8	6.8	0.8	5	1.6	4.8	4.7	1.5	1.6	11.3	3.4	10.5	0	0	0.96	100.42
Interior	98.21	0.17	1.21	0.1	0.1	0.06	0.01	0.11	0.8	41.5	1.8	6.4	1.4	5.3	1.6	2.6	5.4	2.4	1.8	7.1	8.3	15.5	0	0	0.52	100.50
5	96.66	0.53	1.48	0.11	0.08	0.02	0.03	0.19	0.8	41.7	2.5	7	1.7	9	1.5	5.1	5.8	4.2	2.1	9.2	10.8	18.3	2.8	0.3	0.93	100.04
6	97.98	0.6	0.31	0.06	0.05	0.02	0.02	0.16	0.7	31.7	1.7	5.8	0.8	3	0.8	3	5.2	1.7	1.3	8.6	9.5	13.4	0	0	0.34	99.55
7																										
Coating	96.57	1.04	1.58	0.21	0.09	0.06	0.05	0.09	1.6	63.5	3.9	9.5	2	11	2.4	6.3	6.1	6	3.2	10.3	8.5	19.4	13.6	0	1.08	100.78
Interior	96.69	0.88	1.51	0.2	0.12	0.06	0.04	0.09	1.4	57.2	3.4	8.1	0.7	10.6	2.2	6.7	5.7	5	2.2	7.6	10.9	18.6	13.9	0.1	0.77	100.38
GSA																										
Coating	98.7	0.1	0.65	0.07	0.08	0.06	0.01	0.03	0.5	29.9	1.1	6	0.7	3.6	0.5	2.6	5	1.2	2.7	7.3	1.4	6	0	0.3	0.32	100.03
Interior	99.3	0.08	0.54	0.05	0.07	0.05	0.01	0.03	0.6	26.9	1.3	5.7	1.4	2.6	0.9	2.9	4.8	0	2.1	7.9	2.3	5.9	0.2	0	0.22	100.35
ICS																										
Coating	90.21	6.91	0.64	0.08	0.05	0.01	0.13	0.06	1.4	33.3	5.3	7.3	7.5	0	0	12.8	7.7	20.9	4.5	8.8	122.2	80.5	3.6	1.2	1.61	99.73
Interior	97.44	0.37	0.6	0.1	0.06	0	0.02	0.04	0.7	26.8	1.5	6.9	1.4	4.6	1	3.2	5.2	1.3	1.6	6.8	7.1	11.2	4	0	0.36	98.99
RI-1	97.93	0.07	0.38	0.03	0.02	0.01	0.01	0.06	0.2	26.1	0.8	5.1	1.1	1.9	1.2	2.4	4.9	1.7	3	9.5	7.3	6.1	0	0	0.25	98.76
SIB	96.22	0.08	0.66	0.11	0.09	0.01	0.01	0.07	0.6	43.1	1.8	7	1.3	6.2	1.6	1.7	4.5	1.4	1.2	11	4.3	7	2.5	0	0.46	97.72
TOC2	97.45	0.07	0.35	0.06	0.06	0.01	0.01	0.02	0.4	28.3	1	6.1	1.1	3	1	3.8	5.3	0.3	2.3	7.9	2.4	6.6	0	0	0.42	98.46

Table 7. XRD results

Sample ID		Quartz	K-spar	Plagioclase	Goethite	Kaolinite	Smectite	Degree of fit
1B								
	Coating	94.6	3.3	-	-	1.2	0.8	0.1307
	Interior	94.5	4.2	-	-	0.9	0.4	0.1239
3								
	Coating	93.4	2.7	1.2	-	1.1	1.6	0.0994
	Interior	94.5	3.2	1.1	-	0.7	0.4	0.1302
4								
	Coating	95.5	2.8	-	-	1.0	0.6	0.1498
	Interior	95.7	2.4	-	-	1.3	0.7	0.1343
7								
	Coating	94.0	3.5	-	-	0.9	1.6	0.1409
	Interior	94.2	2.9	-	-	1.5	1.3	0.1269
GSA								
	Coating	97.2	1.9	-	-	0.8	-	0.1391
	Interior	92.8	2.9	-	-	1.5	2.8	0.1401
ICS								
	Coating	91.0	2.6	-	3.2	-	3.0	0.0964
	Interior	96.0	1.3	0.9	-	0.7	1.0	0.1683